Carbon Nanotubes

DOI: 10.1002/ange.201305526

"Zero-Dimensional" Single-Walled Carbon Nanotubes**

*Kaladhar Kamalasanan, Riccardo Gottardi, Susheng Tan, Yanan Chen, Bhaskar Godugu, Sam Rothstein, Anna C. Balazs, Alexander Star, and Steven R. Little**

Single-walled carbon nanotubes (SWNTs) are unique, one-dimensional, tubular carbon allotropes with exceptional electronic, mechanical, and transport properties.[1] Individual and dispersible SWNTs are, however, rarely available, as their length and side-wall hydrophobicity drive them to form long bundles.[2] This represents an obstacle[3] in achieving SWNTs of high purity, water solubility, and facile processability for wet nanoscale applications.[4] To date, most dispersion and solubilization strategies rely on chemical functionalization[5] or physical adsorption[6] to introduce sterically demanding groups onto the side walls of the tubes, but the processed tubes generally remain extremely polydisperse, with variable degrees of solubility, and limited processability.[5] If, however, the nanotube length could be reduced to the same order of magnitude as its diameter (thus creating a "zero-dimensional" (0D) carbon nanotube, similar to zero-dimensional fullerenes[7]), the resulting product could retain the desirable properties of a carbon nanotube, but exhibit manageable solubility,[8] thus allowing for better purification and liquid processability. Herein, we describe an iterative, emulsion-based shortening technique for SWNTs that is effective in reducing the length of nanotubes to the same spatial order as their diameter (ca. 1 nm). Combining high resolution transmission electron microscopy (HRTEM) and atomic force microscopy (AFM), we identified and characterized such zero-dimensional carbon nanotubes (0D SWNTs), including their lateral and vertical microscopic signatures. Furthermore, the side walls of 0D SWNTs were functionalized by hydroxylation to achieve durable water solubility (>3 months). Finally, we positively identified these 0D SWNTs using mass spectrometry; to the best of our knowledge, this is the first example of a positive identification of the appropriate signature of a carbon nanotube, using matrix-assisted laser desorption/ionization time-of-flight mass spectrometry (MALDI-TOF-MS). With improved dispersibility and water solubility compared to longer tubes, the 0D SWNTs represent a new, more manageable building block for nanoscale applications. Furthermore, being of the same dimensions as proteins, they are natural candidates for bio-inspired applications.

Our approach to shortening SWNTs is based on the observation that pristine SWNT solubility is extremely limited,[5] and that aggregates of long tubes tend to occupy the oil/water interface in a biphasic solution.[9] Moreover, they have a significant number of local defects along their length (many of which may remain unexposed owing to tube bundling).[10,11] We hypothesized that naturally aggregated SWNTs could debundle/separate in an oil/water emulsion, and possibly orient themselves at that interface, thus facilitating enhanced, and even directional, cutting. Accordingly, we sonicated SWNTs in a biphasic solution (*n*-heptane/water) with a water-soluble oxidant ($KMnO_4$) to help debundle SWNTs. As the oxidant would primarily be present in the water phase, directional oxidation may be possible, initiated by the binding of MnO_4^- to the existing structural defects of the SWNTs.[12] Thus, a tube oriented at an interface may be cut perpendicular to its axis, so that progressively shorter SWNTs are obtained as the procedure is repeated. After eight such oxidative cycles of this emulsion-based method, we observed that complete consumption of the oxidant occurred in less than an hour (6 min for each cycle), as opposed to the several hours of conventional oxidation procedures employing similar oxidants.[13] We ascribe this remarkable effect to improved exposure of the tubes at the interface. Reaction by-products, such as MnO_2, were removed after each cycle. The final product is a transparent, brown aqueous solution that begins to exhibit light precipitation after one day. These results suggest that, after processing, the product exhibits a far greater degree of dispersibility than long, unprocessed SWNTs.

To determine whether the process was successful in producing extremely short carbon nanotubes, we first assessed progressive toluene dilutions of our reaction product by dynamic light scattering (DLS); these tests confirmed their sub-10 nm dimensions (Supporting Information, Figure S1). Samples were then analyzed using HRTEM, which permits visualization with exceptional lateral resolution.[14] At low magnification, HRTEM images revealed that long, unprocessed SWNTs (1 ± 0.22 nm diameter) produced the expected

[*] Dr. K. Kamalasanan,[+] Dr. R. Gottardi,[+] Dr. S. Rothstein, Dr. A. C. Balazs, Dr. S. R. Little
Department of Chemical and Petroleum Engineering, University of Pittsburgh, 3700 O'Hara Street, Pittsburgh, PA 15261 (USA)
E-mail: srlittle@pitt.edi
Homepage: http://littlelab.pitt.edu
Dr. R. Gottardi[+]
Ri.MED Foundation, Palermo (Italy)
Dr. S. Tan
Department of Electrical and Computer Engineering, University of Pittsburgh, 3700 O'Hara Street, Pittsburgh, PA 15261 (USA)
Dr. Y. Chen, Dr. B. Godugu, Dr. A. Star
Department of Chemistry, University of Pittsburgh
219 Parkman Avenue, Pittsburgh, PA 15260 (USA)
[+] These authors contributed equally to this work.

[**] We thank H. Hofer and R. Ridenour for their technical assistance, and Prof. C. Prakash Sharma (SCTIMST, India) and Dr. B. L. Allen (University of Pittsburgh (USA)) for valuable discussions. This work was supported by funding from the National Science Foundation (CDI 0941260) to A.C.B. and S.R.L., and by a Fondazione Ri.MED fellowship to R.G.

Supporting information for this article is available on the WWW under http://dx.doi.org/10.1002/anie.201305526.

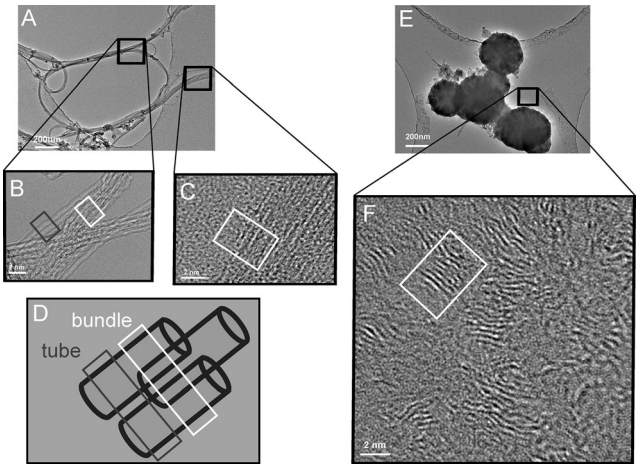

Figure 1. HRTEM images of carbon nanotubes. Tubular macroaggregates on a TEM grid of: A) long, bundled carbon nanotubes suspended across the grid hole (scale bar = 200 nm). B) Long tubes spanning a grid hole (scale bar = 2 nm). C) Long tubes laying on the grid support (scale bar = 2 nm). D) A bundle of tubes as they would appear under an electron beam; the black square indicates how single tubes would appear (spacing on the order of a tube diameter; $d_s = 0.8$–1.2 nm); the white square shows how a bundle of tubes would appear (d_s ca. 0.36 nm). E) Aggregates of short tubes (scale bar = 200 nm). F) Magnified image of aggregates of shortened tubes (scale bar = 2 nm).

bundles, which span across the holes of the supporting grid (Figure 1 A). At higher magnification, SWNTs could be identified as pairs of parallel, dark lines, because the electron beam encounters more carbon atoms when traveling along the tube curvature (Figure 1 B, C, yellow box). These observations are consistent with the literature, suggesting that parallel tightly packed SWNTs appear as close lattice fringes by HRTEM.[15,16] The packing organization follows a hexagonal lattice (a "log-stack" arrangement) with a lattice constant (a), which can be estimated by summing the SWNT diameter and the intertubular spacing, which is due to van der Waals interactions,[17] as $a = 1.32 \pm 0.12$ nm. The corresponding fringe pattern can be calculated by projecting the "shadows" of each overlapping SWNT in the lattice on a plane, thus obtaining a fringe spacing (d_s) of ca. 0.34 nm. Our experimental findings match well with these calculations, as pristine SWNT bundles, both those spanning holes ($d_s = 0.37 \pm 0.16$ nm) (Figure 1 C) and those lying on the supporting grid, ($d_s = 0.36 \pm 0.14$ nm) (Figure 1 D) exhibit this same pattern. Such fringes can be considered as fingerprints for closely packed, overlapping, and (locally) parallel multiple tubes in a hexagonal lattice (Figure 1 C and D). When the product of our cyclic oxidation procedure is examined at low magnification, no such hole-spanning could be identified in the sample, but instead small (< 100 nm) interconnected aggregates were present on the supporting grid (Figure 1 E). Higher magnification HRTEM imaging near the larger aggregates deposited on the grid (Figure 1 E, indicated by the square) revealed a randomly distributed series of close lattice fringes (Figure 1 F) with a spacing of $d_s = 0.36 \pm 0.12$ nm, which is similar to that observed in the case of long overlapping tubes. According to these results, the shortened tubes reside in a mini-bundle, resembling the same log-stack arrangement observed with the long, unprocessed tubes. We observed that the tubes in these stacks are approximately 2–3 nm in length (Figure 1 F), which is now on the same order of magnitude as their diameter.

To further strengthen the microscopic characterization, and to confirm the stacking of the shortened tubes in mini-bundles, AFM imaging was performed. Although objects characterized by AFM suffer from a well-known broadening artifact in the imaging plane owing to the tip size,[18] the vertical resolution of AFM is suitable for precisely determining the height of nanoscale objects. Assuming a minimal energy packing for short tubes (the hexagonal lattice packing of a log-stack arrangement), geometric considerations connect the height of the stack (h) to the radius of a single tube (r) by the relation $h = [2 + (n-1)\sqrt{3}]r$, where n is the number of layers in the stack. When $R > r$ is used to account for the van der Waals intertubular spacing, the relation becomes $h = [2 + (n-1)\sqrt{3}]R$, where $R = a/2$, and a is the hexagonal lattice constant. Thus, if the tubes were assembled into log-stack structures of $n = 1$, 2, 3, or 4 layers, the corresponding height observed by AFM would be $2R$, $3.7R$, $5.5R$, or $7.2R$, respectively (Figure 2). Experimentally, the measured height of a single tube layer ($h_{1\mathrm{exp}}$ ca. 1 nm) is lower than the expected value of $2R = a = 1.32 \pm 0.12$ nm because of the compression exerted by the AFM tip during imaging.[19,20] Correcting for this compression effect, the values for $h_{\min}$ and $h_{\max}$ reported in Figure 2 represent the extreme cases of the h range, and, experimentally, we would expect the heights of the actual tube stacks to fall somewhere in between. Indeed, the experimental height profiles of a well-dispersed population of the shortened tubes are consistent with the expected values for stacks of up to five layers. Representative profiles are shown in Figure 2, and a height-distribution histogram is shown in Figure S2. Notably, above five tubes in a stack, the estimated $h_{\max}$–$h_{\min}$ range becomes too wide, and thus, because of too much overlap between the n and $n+1$ ranges, conclusive statements concerning the bundle order are not possible. Regardless, for stacks that are less than five tubes high, and once the compression of the AFM tip is accounted for, the diameter of the tube bundles, as calculated from the HRTEM, is consistent with the height of the tube bundles suggested by AFM. Accordingly, the high horizontal resolution imaging by HRTEM, and the above AFM data, strongly suggest that the tiny structures present in the solution are in fact crystal-like mini-bundles of short tubes, whose length is in the same order of magnitude as their diameter, that is, they are 0D SWNTs. Considering the good dispersibility of these tubes after the oxidation cycles, it may be that the observed log-stack arrangement occurs mostly during the drying process, which is similar to the assembly of anisotropic particles under a lateral capillary force.

In the long term, complete tube dispersibility is a key requirement for better processability of carbon nanotubes[4,8] and would be necessary to accurately identify carbon nanotubes using mass spectrometry.[6] We observed that, whereas unprocessed long tubes rapidly precipitate when dispersed in water (Figure 3 A a), the extremely short 0D SWNTs appear to form relatively stable vesicles upon agitation of the

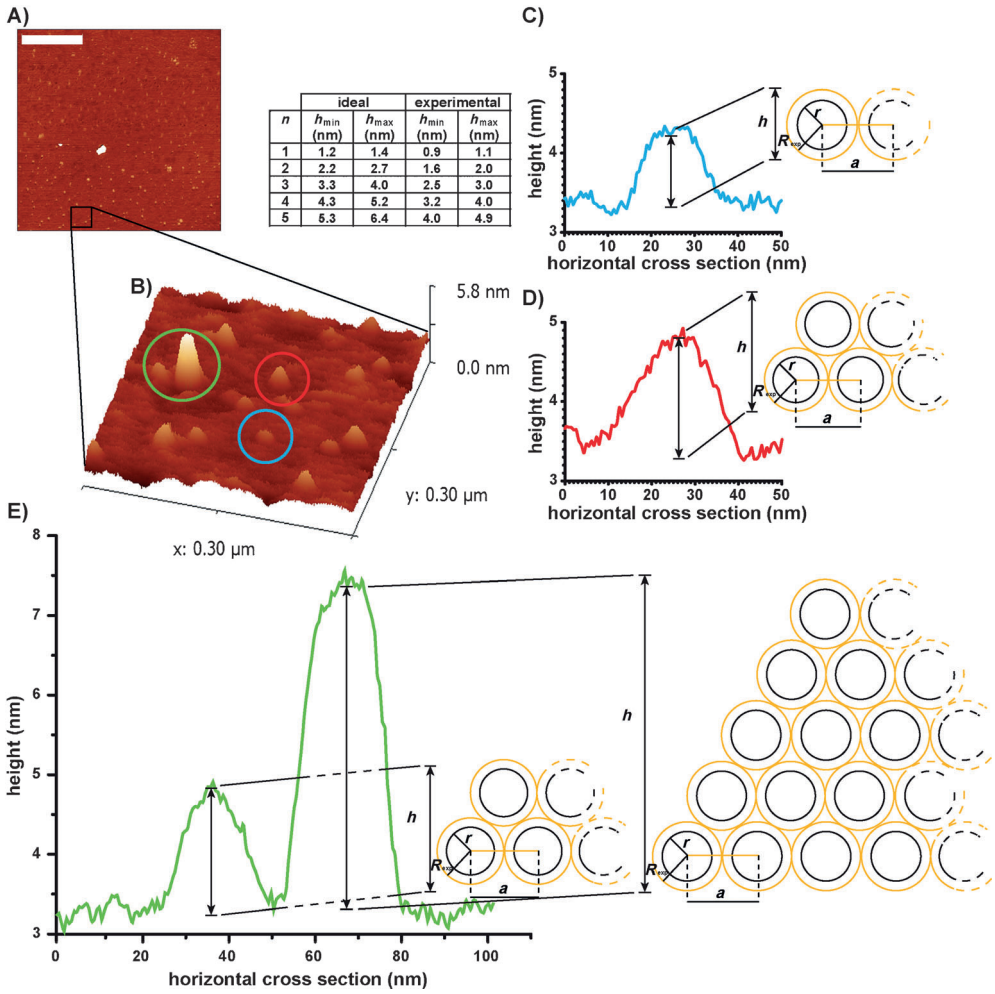

n	ideal h_{min} (nm)	ideal h_{max} (nm)	experimental h_{min} (nm)	experimental h_{max} (nm)
1	1.2	1.4	0.9	1.1
2	2.2	2.7	1.6	2.0
3	3.3	4.0	2.5	3.0
4	4.3	5.2	3.2	4.0
5	5.3	6.4	4.0	4.9

Figure 2. AFM of shortened SWCNTs. A) AFM topographic image of bundles of shortened tubes (scale bar = 1 µm) and B) 3D rendering of a 0.3 µm × 0.3 µm area at higher magnification; the table shows the relation between the number of layers in a stack and the stack height, $h = [2 + (n-1)\sqrt{3}]R$. C, D, E) Cross sections of representative bundles of shortened tubes circled by the corresponding color in (B), compared with the expected height range (table) of bundles formed by $n = 1$–5 layers of stacked short tubes.

n-heptane/water emulsion (Figure 3 A b) and remain in solution for over 24 h. Nevertheless, after that time, a dark brownish precipitate forms in the aqueous phase. Therefore, the side walls of processed nanotubes were modified by hydroxylation, in an attempt to achieve long-term water solubility.[21] Indeed, upon hydroxylation of the side walls (0D OH-SWNTs) with H_2O_2, no precipitate was observed, and the reaction product remained completely soluble in water for over three months (Figure 3 A c).

After good dispersibility in water had been obtained for the processed short tubes, they were spectrally characterized to confirm that 0D SWNTs and the hydroxylated species, 0D OH-SWNTs, indeed maintain the expected spectral properties of intact carbon nanotubes. To this end, UV/Vis/NIR and Raman spectroscopy, which are commonly used to study the structural properties of carbon nanotubes,[22] were employed. Our results suggest that the optical absorption of 0D SWNTs by UV/Vis/NIR spectroscopy is consistent with the one observed for unprocessed SWNTs (Figure 3 B). In particular, the S_{11} peak at 1140 nm presents a small blue shift for 0D SWNTs (dotted line, Figure 3 B), which is similar to what has been described by Sun et al.[23] for fractions of progressively shorter semiconducting nanotubes. The slight difference in baseline intensity for the 0D SWNTs signal (after normalization at 400 nm) is expected as a consequence of the reduction in nanotube length.[24] For the 0D OH-SWNTs, however, the S_{11} signal appears to be attenuated by approximately 80 % (Figure 3 B). As previously shown,[25] this attenuation is a result of side-wall hydroxylation. Accordingly, the degree of substitution with OH groups on the side walls of our completely soluble 0D OH-SWNTs can be roughly correlated to the reduction in the intensity of this peak.[26] Using Raman spectroscopy, both 0D SWNTs and 0D OH-SWNTs exhibit a peak in the radial breathing mode (RBM) region in a similar fashion to unprocessed long tubes (Figure 3 C, insets), which indicates that the tubular structure is maintained after processing. Moreover, 0D SWNTs and 0D OH-SWNTs exhibit the same G and D bands as unprocessed long tubes. The G-band intensity of short tubes is reduced compared to long unprocessed tubes, indicating that the total amount of tubular sp^2 carbon atoms per tube is reduced, which is expected when the tube length is shortened. Overall, the D-band signal, which is characteristic of side-wall defects, remains significantly lower than the G-band signal for all samples, suggesting that the processing introduces only minimal side-wall defects in 0D SWNTs. Furthermore, we observed that the Raman spectrum of 0D OH-SWNT has a sharpened RBM peak (Figure 3 C c, inset), and that the G band is broadened (Figure 3 C c, arrow). These are typical effects of resonance activation of specific Raman peaks, caused by hydroxylation.[17,25] Moreover, for our 0D SWNTs we observed additional radial breathing modes (Figure 3 C b, inset), a phenomenon predicted by Saito et al.[27] for ultra-short nanotubes. Overall, our spectral characterization strongly suggests that the tiny structures have commensurate tubular, structural, and optical properties to the long tubes, and that their side walls remain highly pristine.

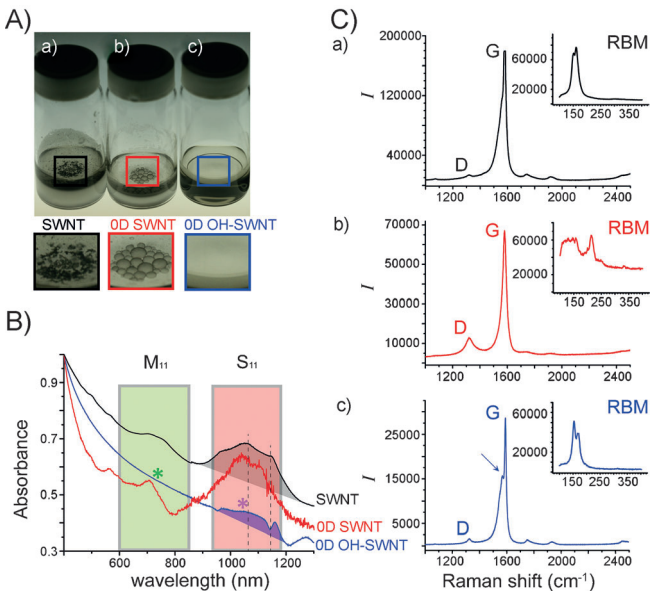

Figure 3. Properties of short nanotubes. A) Solubility/interfacial properties of short nanotubes in hexanes (upper phase) and water (lower phase): a) long tubes, b) short tubes, c) hydroxylated short tubes. The second row of images shows a magnification of the framed area. B) UV/Vis/NIR spectra of nanotubes with shaded regions for metallic (M_{11}-green) and semiconducting (S_{11}-pink) nanotubes. Dotted lines indicate the position of the peaks for SWNTs and the corresponding peaks in 0D SWNTs appear blue shifted. The stars mark the reduction in area under the peak for 0D OH-SWNTs. C) Raman spectra of the tangential mode (G and D Band) and the radial breathing mode (RBM; insets) regions for a) long tubes, b) short tubes, and c) hydroxylated short tubes. The arrow indicates the resonance activation and broadening following hydroxylation.

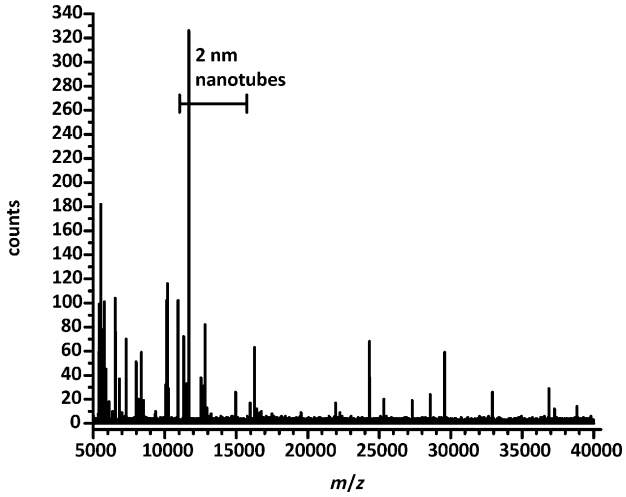

Figure 4. Full MALDI-TOF spectrum of a sample mix of hydroxylated 0D SWNTs at a grid voltage of 92% and a laser intensity of 2104 J cm^{-2}.

Finally, given that our HRTEM data suggest that the 0D SWNTs may actually be in the size range of certain proteins, such as cell-membrane-spanning proteins (2–3 nm long and less than 1.5 nm wide),[28] and that their hydroxylated derivatives, 0D OH-SWNTs, are completely water-soluble and stable, we attempted to characterize 0D OH-SWNTs by MALDI-TOF-MS, a technique widely used to identify intact proteins, polymers, oligomers, and compounds of higher molecular weight.[29] We focused on 0D OH-SWNTs, as their complete solubility and good dispersibility in the MALDI matrix makes them a suitable candidate for MALDI-TOF-MS. Accordingly, we first calculated the hypothetical molecular mass of an ionized 0D OH-SWNT that would be detected by MALDI-TOF, by accounting for its size (as estimated by HRTEM imaging) and the degree of hydroxylation (estimated from the substitution from the S_{11} ($\lambda = 1140$ nm) peak in the UV/Vis/NIR spectrum). The hydroxylated 0D SWNT would then appear as a molecular mass signal $[M+H]^+$ in MALDI-TOF-MS of m/z ca. 11080–15860 for a length of 2 nm. Indeed, after optimizing the extraction parameters to obtain sharp peaks above noise level, the resulting MALDI-TOF-MS peak for 0D OH-SWNTs presents a molecular mass signal of $m/z = 11680$, thus confirming our calculations (Figure 4). Minor peaks are also visible nearby, and they can be ascribed to slightly longer or shorter 0D SWNTs. In general, the peaks observed by MALDI-TOF-MS from a sample comprised of multiple compounds are dependent on the instrumental parameters, such as acceleration voltage, laser intensity, and grid voltage. Thus, the peaks for all compounds are not all visible simultaneously, but as these parameters are adjusted, the different compounds can be progressively extracted, and their respective spectrometric signatures independently recognized. Indeed, the sample of 0D OH-SWNTs analyzed in our study is a mixture of short nanotubes of several different lengths, as suggested in Figure 1. Hence, as we repeated the same test on the same sample, while changing the extraction parameters (acceleration voltage, laser intensity, grid voltage), we observed different sets of peaks, as would be expected for a mixture of different molecules. In Figure S3, the spectrometric signatures between 10000 m/z and 16000 m/z for different combinations of extraction grid voltage and laser intensities are reported, and suggest that each combination extracts 0D OH-SWNTs of slightly different lengths. Importantly, when we analyzed our negative controls (matrix only, without 0D OH-SWNTs), we did not observe any of the sharp peaks presented in Figure 4. The macromolecular mass obtained by MALDI-TOF-MS correlates well with the expected mass of tubes in the length range observed by HRTEM, and with the extent of hydroxylation estimated by UV/Vis/NIR; this suggests that we are indeed observing the mass spectrometric signature of 0D OH-SWNTs. To the best of our knowledge, this is the first report of a mass spectrum of carbon nanotubes that correlates well with the microscopic signatures of the tubes. Accordingly, MALDI-TOF-MS, in conjunction with initial HRTEM and AFM size characterization, may become an extremely sensitive detection method for nanotubes and their complexes in such different environments as cell lysates, cell/tissue culture media, and blood, much as proteins and fullerenes are currently detected.[30]

In conclusion, we have demonstrated the successful production and characterization of zero-dimensional carbon nanotubes. We have also shown that they can be fully solubilized in water by side-wall functionalization with very

low side-wall defects. With better dispersibility and water solubility than longer tubes, the 0D SWNTs could be used as new, more manageable building blocks for a number of nanoscale and bio-inspired applications. Furthermore, such short tubes now appear to have the same dimensions as proteins, such as membrane-spanning proteins, making them natural candidates for peptide carriers for vaccine or drug delivery, vectors for gene transfection, and even insertion into lipid bilayers to serve as new candidates for synthetic transmembrane channels.[31,32]

Received: June 27, 2013
Published online: September 5, 2013

Keywords: dispersibility · functionalization · mass spectrometry · nanotechnology · nanotubes

[1] R. H. Baughman, A. A. Zakhidov, W. A. de Heer, *Science* **2002**, *297*, 787 – 792.
[2] P. K. Rai, R. A. Pinnick, A. N. G. Parra-Vasquez, V. A. Davis, H. K. Schmidt, R. H. Hauge, R. E. Smalley, M. Pasquali, *J. Am. Chem. Soc.* **2006**, *128*, 591 – 595.
[3] M. J. O'Connell et al., *Science* **2002**, *297*, 593 – 596.
[4] H. Murakami, N. Nakashima, *J. Nanosci. Nanotechnol.* **2006**, *6*, 12.
[5] J. Chen, M. A. Hamon, H. Hu, Y. Chen, A. M. Rao, P. E. Eklund, R. C. Haddon, *Science* **1998**, *282*, 95 – 98.
[6] M. Holzinger, J. Abraham, P. Whelan, R. Graupner, L. Ley, F. Hennrich, M. Kappes, A. Hirsch, *J. Am. Chem. Soc.* **2003**, *125*, 8566 – 8580.
[7] A. K. Geim, K. S. Novoselov, *Nat. Mater.* **2007**, *6*, 183 – 191.
[8] Z. Chen, K. Kobashi, U. Rauwald, R. Booker, H. Fan, W.-F. Hwang, J. M. Tour, *J. Am. Chem. Soc.* **2006**, *128*, 10568 – 10571.
[9] H. Wang, E. K. Hobbie, *Langmuir* **2003**, *19*, 3091 – 3093.
[10] Y. Fan, B. R. Goldsmith, P. G. Collins, *Nat. Mater.* **2005**, *4*, 906 – 911.
[11] K. Suenaga, H. Wakabayashi, M. Koshino, Y. Sato, K. Urita, S. Iijima, *Nat. Nanotechnol.* **2007**, *2*, 358 – 360.
[12] J. Zhang, H. Zou, Q. Qing, Y. Yang, Q. Li, Z. Liu, X. Guo, Z. Du, *J. Phys. Chem. B* **2003**, *107*, 3712 – 3718.
[13] J. Liu et al., *Science* **1998**, *280*, 1253 – 1256.
[14] R. R. Schlittler, J. W. Seo, J. K. Gimzewski, C. Durkan, M. S. Saifullah, M. E. Welland, *Science* **2001**, *292*, 1136 – 1139.
[15] J.-F. Colomer, L. Henrard, P. Lambin, G. Van Tendeloo, *Eur. Phys. J. B* **2002**, *27*, 111 – 118.
[16] A. Thess et al., *Science* **1996**, *273*, 483 – 487.
[17] *Physical Properties Of Carbon Nanotubes* (Eds.: R. Saito, G. Dresselhaus, M. S. Dresselhaus), Imperial College Press, New York, **1998**.
[18] C. Canale, B. Torre, D. Ricci, P. C. Braga in *Atomic Force Microscopy in Biomedical Research* (Eds.: P. C. Braga, D. Ricci), Humana, Totowa, NJ, **2011**, pp. 31 – 43.
[19] A. Almaqwashi, J. W. Kevek, R. M. Burton, T. DeBorde, E. D. Minot, *Nanotechnology* **2011**, *22*, 275717.
[20] T. DeBorde, J. C. Joiner, M. R. Leyden, E. D. Minot, *Nano Lett.* **2008**, *8*, 3568 – 3571.
[21] R. S. Pantelic, J. W. Suk, Y. Hao, R. S. Ruoff, H. Stahlberg, *Nano Lett.* **2011**, *11*, 4319 – 4323.
[22] T. Belin, F. Epron, *Mater. Sci. Eng. B* **2005**, *119*, 105 – 118.
[23] X. Sun, S. Zaric, D. Daranciang, K. Welsher, Y. Lu, X. Li, H. Dai, *J. Am. Chem. Soc.* **2008**, *130*, 6551 – 6555.
[24] J. A. Fagan, J. R. Simpson, B. J. Bauer, S. H. D. P. Lacerda, M. L. Becker, J. Chun, K. B. Migler, A. R. H. Walker, E. K. Hobbie, *J. Am. Chem. Soc.* **2007**, *129*, 10607 – 10612.
[25] M. S. Strano, C. A. Dyke, M. L. Usrey, P. W. Barone, M. J. Allen, H. Shan, C. Kittrell, R. H. Hauge, J. M. Tour, R. E. Smalley, *Science* **2003**, *301*, 1519 – 1522.
[26] S. Wang, P. He, J.-M. Zhang, H. Jiang, S.-Z. Zhu, *Synth. Commun.* **2005**, *35*, 1803 – 1808.
[27] R. Saito, T. Takeya, T. Kimura, G. Dresselhaus, M. S. Dresselhaus, *Phys. Rev. B* **1999**, *59*, 2388 – 2392.
[28] A. Poetsch, D. Schlüsener, C. Florizone, L. Eltis, C. Menzel, M. Rögner, K. Steinert, U. Roth, *J. Biomol. Techn.* **2008**, *19*, 129 – 138.
[29] M. Lin, J. M. Campbell, D. R. Mueller, U. Wirth, *Rapid Commun. Mass Spectrom.* **2003**, *17*, 1809 – 1814.
[30] B. Belgorodsky, L. Fadeev, J. Kolsenik, M. Gozin, *ChemBioChem* **2006**, *7*, 1783 – 1789.
[31] M. Dutt, O. Kuksenok, S. R. Little, A. C. Balazs, *Nanoscale* **2011**, *3*, 240 – 250.
[32] M. Dutt, O. Kuksenok, M. J. Nayhouse, S. R. Little, A. C. Balazs, *ACS Nano* **2011**, *5*, 4769 – 4782.